Central Power Research Institute

Power Research

Development of a Self-Powered Temperature Monitoring Wireless Node for Transmission Lines for Smart Grid Application

Atulya Mishra* and J. Sundara Rajan

CPRI, Bangalore - 560080, Karnataka, India; er.atulya@gmail.com

Abstract

Increasing the safe operating temperature limits of the transmission line, by a small percentage above the present safe operating temperature limit can help in transmission of more power over existing lines and it would also help in avoiding huge investment and loss of time due to regulatory processes for establishment of new lines. Since the operating temperature is a critical parameter for transmission of the power, low cost sensors on high tension lines would enable data acquisition on real time basis for faster decision making. This is an alternative power source to the battery or solar panels. The results of laboratory experiments and data on simulation for the developed self-powered temperature, sag and tension monitoring system are presented and discussed in this paper. A comparison of two different methods of computation of temperature based on frequency and amplitude of output signal and cost benefit of the different methods of powering the wireless sensor nodes for transmission line application are also discussed.

Keywords: Energy Harvesting, Temperature Monitoring System (TMS), Thermal Limit, Sensitivity, Xbiee

1. Introduction

The maximum loading capability of power transmission line is determined by the system stability, permissible voltage regulation and thermal limit of the conductors[1,2]. Among these operational parameters, the thermal limit depends on both operations of transmission line as well as ambient conditions. For a given transmission line conductor, there are two parameters that are very important form the point of temperature. These are the operating limits[3] (which is decided by regulatory authority) and the thermal limit[4] (which depends on conductor design and material). Thermal limit of a conductor is associated with the steady-state and overload conditions. It is the maximum temperature at which a conductor can operate continuously by maintaining its tensile strength[4] within the safe limits as recommended by the manufac-

turer. Therefore, the thermal limit of conductor is higher than the operating limit and a cross over beyond this limit would reduce the mechanical strength of conductor due to annihilation, which is 93°C for aluminum[3]. The typical thermal limits of different grades of conductors are shown in Table 1.

Table 1. Maximum conductor temperature limits[3]

Conductor material	Temperature limits	
	Normal rating(°C)	Normal rating(°C)
ACSR, steel >= 7.5% area	93	93
ACSR, steel < 7.5% area	93	93
AAAC,AAC, & ACAR	93	93
ACSS, steel >= 7.5% area	200	200
Copper	75	75

---

*Author for correspondence

Limit of the conductor has been set at 65˚C[1,2,5]. However, by increasing the safe operating thermal limit of the conductor to 85˚C, would help in transmission of more power to the load centres. It is estimated that on allowing conductor temperature to rise by every one degree above 65˚C (which is the present safe thermal operating limit), there is a possibility of transmitting an extra 6.5 MW of power in a 400 kV system when ambient temperature is at 40˚C. Since temperature of the conductor as well as local ambient temperatures *play* a critical role in power transmission capability, there is a need for a sensitive Temperature Monitoring System (TMS) which can be integrated to a communication facility for online monitoring of the temperature of the transmission line. Since tension and sag of the conductors depend on temperature, a Sag and Tension Monitoring System (STMS) along with temperature sensor is also essential for the transmission lines.

In the designed Temperature Monitoring System (TMS) and Sag and Tension Monitoring System (STMS), the sensor unit will be fixed on the conductor. The sensor unit measures the temperature, tension and sag of conductor and communicates the measured data at a predetermined time interval to a base station on the tower. To energize the monitoring system an energy harvester system has been designed and this system harvests energy[14–24] from magnetic field of the conductor.

This paper discusses the experimental and simulation results of the developed compact, reliable, all weather proof TMS and its extension to STMS. Two different methods of measurement of temperature, one based on variations in amplitude and other using variations in frequency of the signal are discussed. The cost comparisons of battery powered, solar powered and energy harvester powered wireless monitoring systems are compared to highlight the advantages of the proposed energy harvester.

2. Theoretical Background

2.1 Effect of Weather on Power Transmission Capacity

The electrical conductors are designed to a 'rated ampacity', which is the maximum current the conductor is capable of carrying under standard ambient temperature and wind

conditions[6,7]. Increase in ambient temperature will reduce the ampacity of transmission line conductor due to reduction in its ability to dissipate heat[7]. In winter season, when the ambient temperatures are low, there is better heat dissipation from the conductor and hence, larger current can be carried by the conductors. In summer, the difference in ambient temperature and the maximum operating temperature is reduced, and hence the current carrying capability of the conductor reduces correspondingly. To understand the reductions in the ampacity of the conductor under fluctuating weather conditions, the thermal energy balancing model is used. The dynamic energy balance of overhead power line is given by equation:

$$\Delta \dot{E} = \dot{q}_j + \dot{q}_s - \dot{q}_c + \dot{q}_d - \dot{q}_r \qquad (1)$$

Under steady state condition, $\Delta \dot{E} = 0$ and $\dot{q}_d = 0$ since there is no conduction of heat.

$\dot{q}_c$ heat dissipation due to convection over a length of one meter of the conductor.

$\dot{q}_r$ heat emission due to radiation from one meter long conductor.

$\dot{q}_j$ generation of heat due to current flow in conductor per meter length of the conductor.

$\dot{q}_s$ solar heat gained per meter of length of the conductor.

For equilibrium conditions in the system, total heat input to the conductor must be equal to total heat transfer out of the conductor.

$$\dot{q}_c + \dot{q}_r = \dot{q}_j + \dot{q}_s \qquad (2)$$

Increasing in heat due to electrical loading is dependent on current transmitted through the conductor (I) and resistance of the overhead conductor (R) at a given temperature[7] according to the Equation:

$$\dot{q}_j = I^2 R \qquad (3)$$

Rearranging the terms in the heat balance equation, the maximum allowable current in a conductor is given by

$$I = \sqrt{\frac{\dot{q}_c + \dot{q}_r - \dot{q}_s}{R}} \quad \text{at constant temperature} \quad (4)$$

The expanded form of rated ampacity of an overhead conductor can be expressed in terms of weather parameters (ambient temperature, wind speed, solar insolation), conductor properties (diameter, surface area, material properties) and can be expressed using the equation

$$I = \sqrt{\dfrac{\pi.h.D.(T_{conductor} - T_{ambient}) + \pi.\in.\sigma.D(T_{conductor}{}^4 - T_{ambient}{}^4) - \delta.D.a_s}{R}} \qquad (5)$$

Here

h average heat transfer co-efficient

D conductor diameter

$T_{ambient}$ ambient temperature

$\in$ emissivity of conductor surface

σ Stefan-Boltzmann constant

δ incident solar radiation

a_s absorptivity of conductor surface

2.2 Effect of Weather Condition on sag of the Transmission Line

Maximum thermal operating temperatures for conductors are defined to ensure compliance with air clearance from the ground level along with guide lines, in addition to avoiding mechanical damage of the conductors and line hardwire parts[8]. For a typical Aluminum Conductor with Steel-Reinforcement (ACSR), the maximum allowable operating temperatures may vary from 50˚C to 180˚C, depending on the engineering practices, tolerance and the duration of thermal exposure[7]. When transmission line conductors are operated beyond the maximum operating temperature, it results in additional sag and loss of mechanical strength[7]. To avoid increase in maximum thermal operating limit of the line, the operators usually limit the current flow in the conductor to be well within the thermal limits[6,7]. The increase in temperature of the conductor causes elongation in the conductor, which in turn increases the sag[9] according to the Equation:

$$\frac{\Delta L}{L} = \alpha \Delta T_c \qquad (6)$$

Here α is the coefficient of linear thermal elongation and it depends on the ratio of aluminum-to-steel surface area and it is specific to each transmission line. Due to the property of the material, aluminum elongates twice in comparison to steel[9]. Therefore, aluminum suffers a larger thermal expansion and contributes significantly towards sag.

3. Description of the TMS

3.1 Components of TMS

The developed TMS consists of an online sensor and a communication unit, which is fixed on the transmission line conductor and a local communication module which is fixed at the base of the tower. This local communication module, at base of the tower, communicates with the communication module, which is fixed on the transmission line conductor. The system components of the designed TMS for transmission line are shown in Figure 1(a).
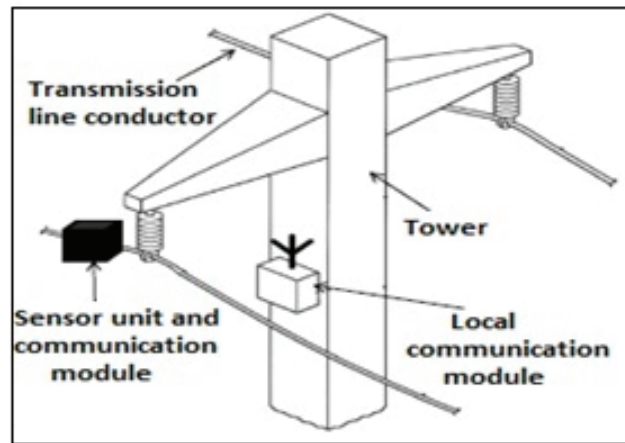
3.2 Electronics of TMS

There are two major units in a TMS namely the sensor/ communication module which is fitted on the transmission line and a local base station at the base of the tower. Inside the sensor and communication unit, a temperature sensing element with required electronic signal conditioning circuits are placed. In this case, a PT100 sensing element is used. Whenever there is a change in temperature, the resistance of PT100 sensor would change leading to either change in amplitude or change in time period of the signal generated at the output of the electronic circuit. Hence, measuring the variation in either of the two quantities i.e. signal amplitude or signal frequency and comparing them with the corresponding reference value of amplitude and time period would give the actual value of the temperature. A conceptual representation of the sensor and communication unit is shown in Figure 1(c).

For measurement of the variations in amplitude of the signal, a wheat-stone bridge and instrument amplifier circuit are used in the circuit and for measurement of the variations in frequency; a two stage oscillator circuit is used. A microcontroller unit is integrated in the electronics for performing the internal mathematical operation and calibration followed by data transmission. A block diagram of the proposed TMS is shown in Figure 1(b) depicting different blocks used in the sensor and communication unit of the TMS.

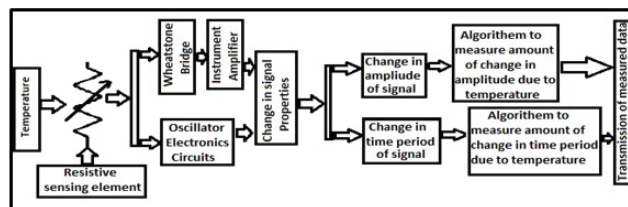## 4. Assessment of Electronic Circuit of TMS by Simulation

In the simulation, a PT100 temperature sensor is used and its resistance is varied to respond the changes in temperature.

(a)
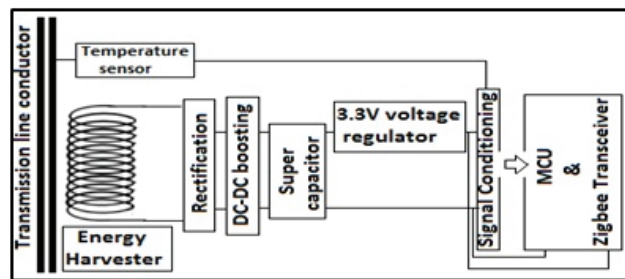
(b)

(c)

Figure 1. Components of TMS. **(a)** System components of online temperature monitoring system (TMS); **(b)** Schematic of the developed TMS; **(c)** Conceptual block diagram of the electronics of the sensor and communication unit.

The change in resistance modifies either the amplitude or the frequency of the output signal. The variations in either of these two electrical parameters are measured to determine the changes in the temperature. Two methods of temperature measurement based on the amplitude variation and frequency variations are discussed in this paper.

4.1 Temperature Measurement using Frequency Method

The circuit of this method consists of a two stage opamp circuit as shown in Figure 2(a) used for conversion of temperature to frequency. A PT100 sensing element is connected to the positive terminal of the 2nd stage of the opamp.

For both simulation and experimental measurements, MCP604 opamp was used. A 3-pin regulator LT1083 was used for control of the output voltage to 3.3 V. Resistance of the PT100 element is varied from 100 to 200 Ω in steps of 10 Ω each. For simulation, LT spice and Proteous 8.4 simulators were used. Figure 2(b) shows the linear relationship between change resistance and change frequency for frequency method. The results of simulation depicting the variation in time period with constant amplitude due to changes in resistance of PT100 is shown in Figure 2(c).

Table 2 shows the dependence of output frequency on resistance of PT100 element when temperature to frequency converter circuit is used. Here the data is transmitted using UART module of PIC16F1936 controller to the remote host receiver module. In Proteous 8.4 simulator, a virtual window terminal was used as the receiver unit for receiving and displaying of the results. The data received at the virtual terminal is in the form of hexadecimal numbers, and it is presented in Table 2.

Table 2. Data of the receiver window of the simulator

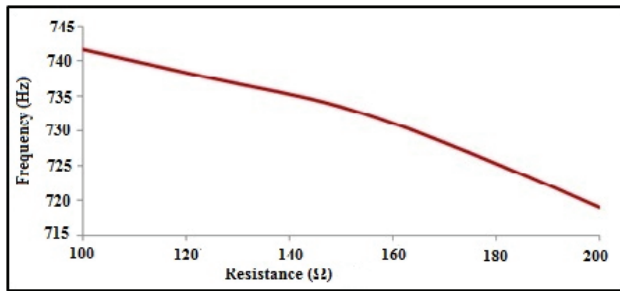| Change in resistance due to temperature effect (Ω)	Variation in output frequency due to temperature effect(Hz)	Data received at virtual terminal window of simulation
110	739.929	0523
120	738.299	064A
130	736.679	0770
140	735.069	0897
150	733.454	09BE
160	730.814	0AE4
170	728.174	0C0A
180	725.281	0D30
190	722.172	0E57
200	719.041	0F7E

The variation in frequency for different values of resistances are shown in Figure 2(c) and it is observed from figure that amplitude of signal remained constant but frequency of the signal changed when there is a change in resistance of PT100. It is also observed that with increasing in resistance due to increase temperature, there is a corresponding fall in the output frequency of the sensor

module. This variation in the output frequency is measured using the microcontroller unit.

It is also observed that with increasing in resistance due to increase temperature, there is a corresponding fall in the output frequency of the sensor module. This variation in the output frequency is measured using the microcontroller unit.
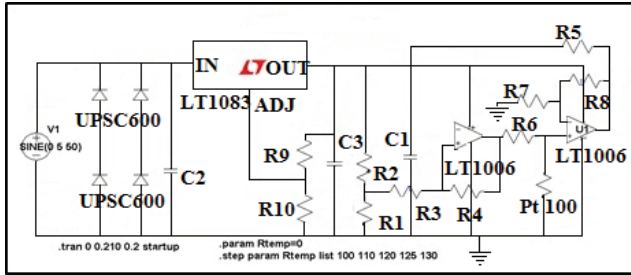
(a)



(b)
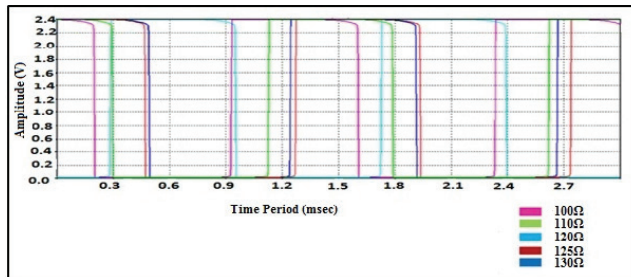
(c)

Figure 2. Temperature measurement by frequency method. **(a)** Circuit for temperature to frequency conversion; **(b)** Variation in output frequency of the sensor node with respect to variations in PT100 resistance due to changes in temperature; **(c)** Results of simulation showing the effect of variations in PT100.

4.2 Flow Diagram for Temperature Measurement by Frequency

In this method, CCP (Capture/Compare/PWM) module of PIC16F1936 controller is used[11]. The CCP module helps in capturing the input signal based on the edge

selection (rise/fall/level). On arrival of the first edge of the input signal at input pin of the controller, ISR (Interrupt Service Routine) is invoked and the timer1 module data is loaded to the CCPR resistor[11]. A similar action takes place on the arrival of the second edge of the input signal. Therefore, the difference between two consecutive values of CCPR register correspond to the difference in time period between two consecutive edge of signal, which is the time period of the signal and reciprocal of it gives the frequency of the signal.

UART module and TXREG register[12] of Pic16F1936 are used for serial communication of temperature data of conductor to remote computer. For this particular application Xbiee communication protocol[10] is used. The flow diagram for the temperature measurement using frequency method is shown in Figure 3
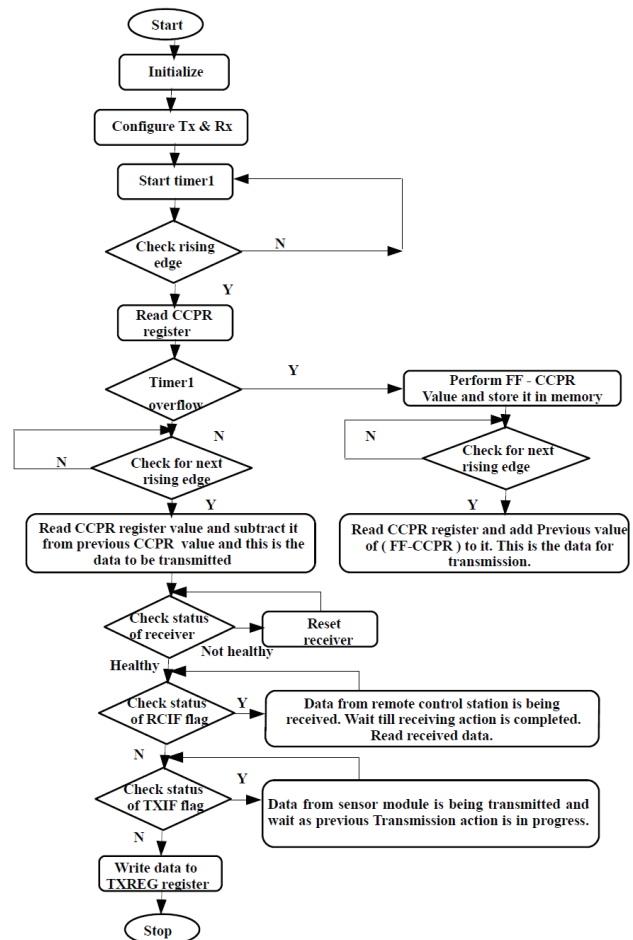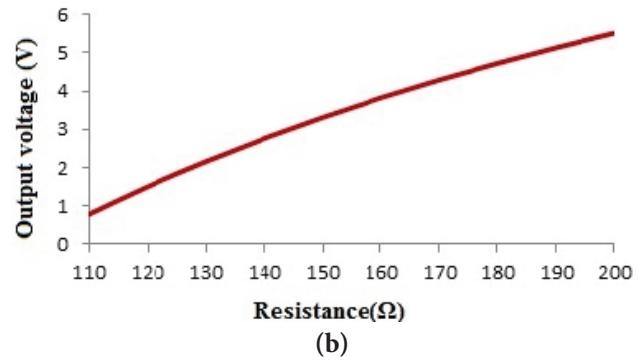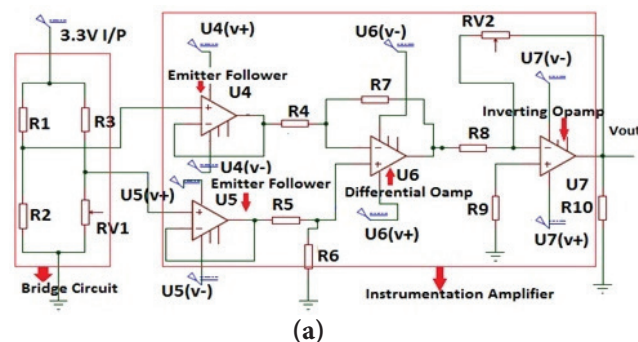

Figure 3. Flow diagram of temperature measurement using frequency method.

4.3 Temperature Measurement Using Amplitude Method

In this approach, a wheatstone bridge circuit is used, which remains at balanced position when PT100 resistance is at 110 Ω. When there is change in temperature, the resistance of the PT100 element changes and the bridge balance condition is disturbed. It is well known that the output of the wheatstone bridge under balance state generates zero output voltage[12]. During the unbalanced condition, the output voltage that is generated is proportional to the change in the value of the resistance of the bridge. The output voltage of the bridge circuit is further amplified to the desired range by using an instumentation amplifier circuit as shown in Figure 4(a). For simulation, the resistance across RV1 was varied at an interval of 10 Ω from 110 Ω to 200 Ω and results are shown in Table 3. The corresponding output voltage of the electronic circuit and the data unit received for variations in resistance is shown in Table 3 in hexa decimal format. The variation of output voltage with respect to resistance is shown in Figure 4(b).

**Table 3.** Data of receiver window of the simulator

Change in resistance due to effect of temperature (Ω)	Change in output voltage due to temperature effect(V)	Data received at virtual terminal window of simulation
110	0.79	0F B0
120	1.51	01 E0
130	2.16	02 AE
140	2.76	03 6C
150	3.31	04 1B
160	3.82	04 BD
170	4.29	05 52
180	4.72	05 DA
190	5.13	06 5D

(a)

(b)

Figure 4. Temperature measurement using amplitude method. **(a)** Circuit for temperature to amplitude conversion; **(b)** Variation of output voltage of sensor node with the variations in the resistance of PT100 using the amplitude method.

4.4 Flow Diagram for Temperature Measurement by Amplitude Method Using TMS

In this method, an ADC module is used to measure the amplitude of the signal and the sensitivity of ADC to get the actual amplitude of the signal. For communication of the data to the remote computer, UART module and TXREG register were used in the prototype of TMS. The flow diagram for the temperature measurement by amplitude method is shown in Figure 5.
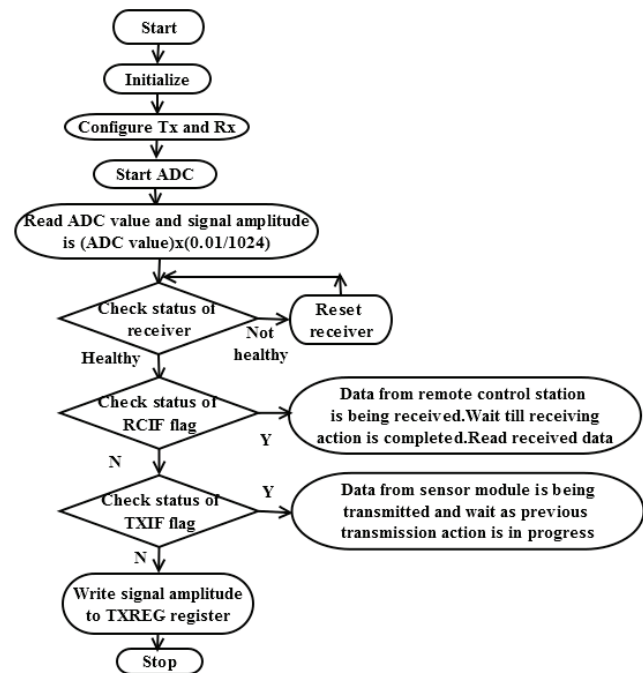
Figure 5. Flow diagram of temperature measurement method using amplitude method.

5. Experimental Results

For the development of a fully functional TMS unit for transmission line temperature measurement, the work was divided into three parts.

In first part a prototype electronic module was fabricated using temperature to frequency converter circuit and the corresponding algorithm was implemented in the controller. The output of the electronic module was tested and results were validated by powering it through an external DC source. In second step, an energy harvester was designed to supply 3.3 V, 156 mA current for powering the electronics of the TMS and the results were verified by varying the conductor current from 50 to 240 A. In the third step both TMS electronics module and energy harvester were integrated and the functionality of electronics of TMS was validated by powering it through energy harvester unit. The details of these three steps are discussed in the sections to follow.

5.1 Validation of Performance of TMS

A prototype electronic module was fabricated to transmit the temperature of conductor, using the temperature measurement by frequency method and the test setup for validation of results of the prototype electronic module is shown in Figure 6.

For the purpose of verification of the results of the prototype, it was powered from a 0-12 A, 0-24 V variable dc source (in place 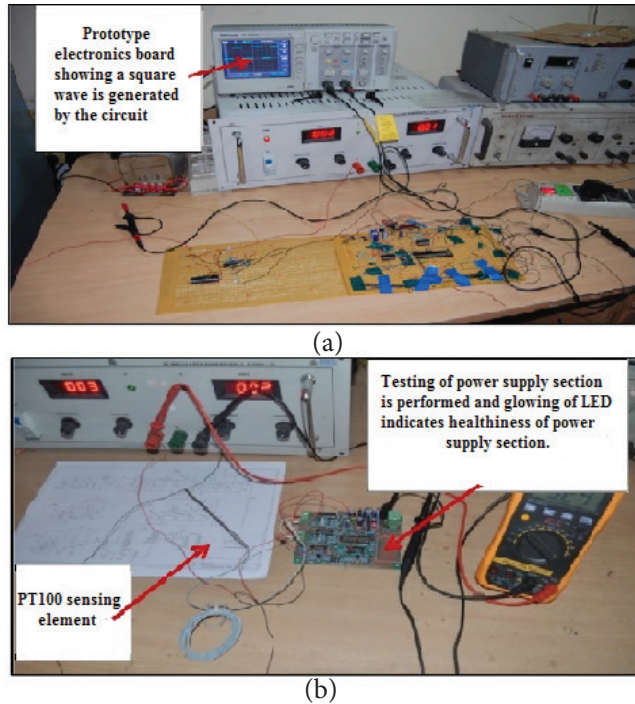of energy harvester) in the laboratory and an oscilloscope was connected across the output of as shown in Figure 6(a). The output of temperature to frequency converter circuit is a square wave with constant amplitude and varying time period as shown in Figure 6(a).

A PT100 sensor was integrated into the electronic module for sensing the temperature of the conductor which was heated by an external heat source and the variations in resistance across the PT100 element due to temperature was recorded by using a digital-meter and corresponding frequency was recorded through an oscilloscope. The results of experiments and simulation are compared in Table 4 (see appendices). It is observed that the deviation of resistance in experiment and simulation are about 0.6 Ω which corresponds to 2°C variation in temperature.

After verification of the functionality of temperature to frequency converter circuit a fully functional PCB was designed using a microcontroller unit (PIC16F1936), a communication module (Tarang P-20 RF module[13]) and the temperature to frequency convert circuit. This circuit was also integrated with an inductive charge booster which boosts dc voltage from 0.5 to 3.3V. At the output of power supply section a LED was connected for indication of healthiness of power supply (i.e., 3.3V, ± 2%) . The photograph of the set up for testing of the power supply section of PCB is shown in Figure 6(b).

Table 4. Comparison of experimental data and results of simulation using the temperature to frequency conversion method

Temperature (°C)	Change in resistance due to temperature effect (Ω)		Difference in resistance from simulation and experimental results (Ω)	Variation in output frequency due to temperature effect(Hz)		Difference in frequency from simulation and experimental results (Ω)
	Experimental results	Simulation results		Experimental results	Simulation results	
28	112.12	110	2.12	738.9	28	112.12
50	119.43	120	-0.57	737.4	50	119.43
80	131.51	130	1.51	734.6	80	131.51
100	140.71	140	0.71	734.9	100	140.71
130	149.23	150	0.77	732.5	130	149.23
158	162.24	160	-2.24	731	158	162.24
188	168.35	170	1.65	727.1	188	168.35
208	181.21	180	1.21	723.9	208	181.21

(a)

(b)

Figure 6. Validation of performance of TMS. **(a)** Photograph of the sensor electronics module for frequency method, showing a square wave is generated by the module; **(b)** Photograph showing the testing of the power supply section of sensor electronic module.

5.2 Development of Energy Harvester Unit for Powering the TMS

After fabrication of all electronics of TMS module the design of energy harvester module was taken up. Two rectangular ferrite bars of dimension of 97.5mm x 35mm x 5mm and a U-shaped lamination of dimension 140mm x 80mm x 4mm were used in the design of the energy harvester. The rectangular ferrite bars are placed on the both sides of the conductor and the U-shaped lamination was fixed across the ferrite bars from the bottom side of the conductor. Copper wire of 42 gauge and 2500 turns were wound around the U-shaped lamination. In the designed energy harvester the rectangular ferrite bar acts as a flux collector and the U-shaped lamination provides a low reluctance path towards the coil. The energy harvester unit was used to power the electronics of TMS in the experimental set up for transmission of temperature of the conductor. A photograph of the developed TMS for transmission line along with the energy harvester, are shown in Figure 7.
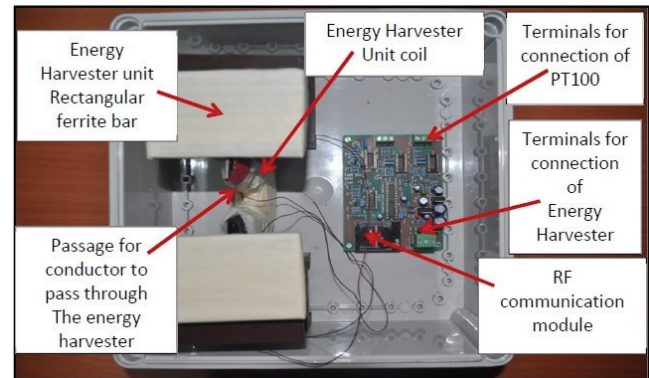
Figure 7. Photograph of developed TMS unit with energy harvester.
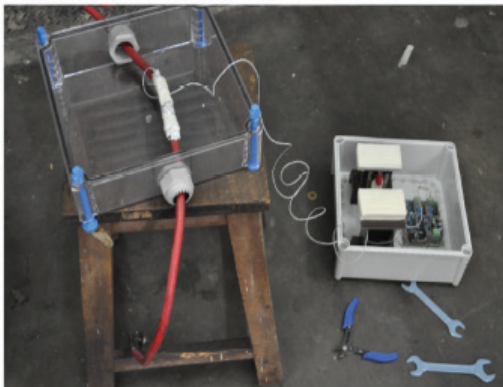
5.3 Experimental Results

It was difficult to replicate the exact transmission line model in the laboratory for loading the line with different magnitudes of ac current.

Hence, a low voltage, high current variable ac current source of 1000 kVA capacity was used for generating currents. Copper conductors of 35 mm2, 50 mm2 were used for experiment purpose. Conductor was connected across the output terminals of the low voltage, high current source and the energy harvester module was fixed to the conductor as shown in Figure 8. An alternating current of magnitude from 50 to 240 A was passed through the conductor and current was increased in steps of 10 A and maintained for 4 to 6 hours for reaching the steady conditions. The wireless sensor node was programmed to transmit the temperature of conductor at intervals of 1 min and a computer was used for receiving and recording of the data. A receiver module was connected to the serial port of the laptop and data was recorded using the TMFT software. The data recorded by the computer is shown in Table 5.

Table 5. Experimental results showing the data recorded by the remote computer corresponding to each line current in the hexa decimal format

Primary line current(A)	Data recorded by remote computer in hexa decimal format
50	03 72
60	03 76
70	03 77
80	03 7A
90	03 7D

Primary line current(A)	Data recorded by remote computer in hexa decimal format
100	03 80
110	03 81
120	03 83
130	03 84
140	03 87
150	03 8C

Figure 9. Variations in the data recorded at remote computer with respect to variation in the line current.

Table 6. Variations in the conductor temperature corresponding to line current at an ambient temperature of 23°C

Primary line current(A)	Conductor temperature (°C)
50	29
60	29.5
70	30
80	30.5
90	31
100	32
110	32.5

Table 6 also shows the temperature data received at the remote terminal of the computer. From Figure 9 it is observed that the data received at the remote computer is nearly linear with respect to variations in the line current. The linearity was further improved by using calibration of data at the software level. From the experimental and simulation results it follows that

- There is an average deviation of 1.5 Hz in experimental results as compared to results of simulation. This deviation arises mainly, because of the resistance values in the experimental approach, do not match the resistance value considered in simulation. The deviation in resistance value between simulation and experiment is around 1.9 Ω.
- The performance of energy harvester and charge pump unit were also verified. It is observed that energy harvester along with charge pump unit, works satisfactorily by supplying 3.3 V and 156 mA for line current of 50 A on-words.
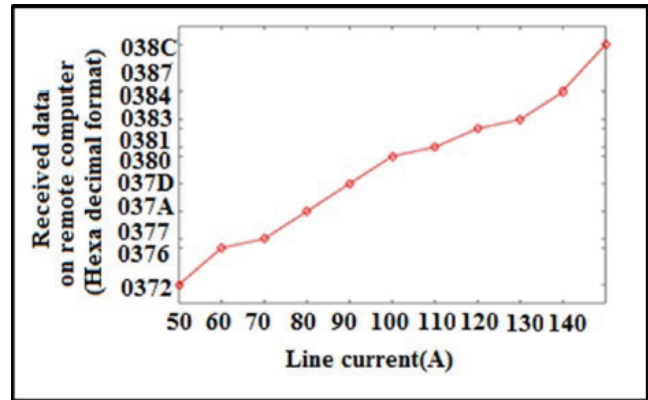

Figure 8. Experimental set up for TMS for validation of result. **(a)** Photograph shows sensing element connected to connector; **(b)** Photograph shows multimeter showing developed e.m.f; **(c)** Photograph shows remote computer receiving data from TMS module.

- The temperature data from TMS was communicated to remote computer, and recorded at TMFT software in the remote computer. The temperature data recorded at remote computer for different line current magnitude and it was observed that the variation in conductor temperature and line current is almost linear.

5.3.1 Sensitivity of Measurement

Temperature measurement using frequency method

The following equations are used for calculation of sensitivity:

$$Sensitivity(S) = \frac{\Delta Output}{\Delta Input}$$

$$S = \frac{\Delta Output\ voltage}{\Delta Input\ Resistance\ due\ to\ temperature}$$

$$= \frac{738.299 - 739.929}{120 - 110} = 0.163 \frac{Hz}{\Omega}$$

Temperature measurement using amplitude method

The following equations are used for calculation of sensitivity:

$$Sensitivity(S) = \frac{\Delta Output}{\Delta Input}$$

$$S = \frac{\Delta Output\ voltage}{\Delta Input\ Resistance\ due\ to\ temperature}$$

$$= \frac{1.51 - 0.79}{120 - 110} = .072 \frac{V}{\Omega}$$

It is important to note that in sensitivity calculation the sensitivity of CCP and ADC module of controller are not considered. Considering the complexity of implementation of algorithms, for the method of temperature measurements by variation in amplitude is easier to implement as compared to the method of temperature measurement by variation in output frequency because in former case ADC and UART module are required to be configure.

6. Conclusion

The important conclusions of this study are as follows:

- An online Temperature Monitoring System (TMS) has been successfully developed and its performance is observed to be satisfactory.
- Two methods of computation of temperature,one using the amplitude and the other one using the frequency have been evolved.It is observed that the sensitivity of the circuit used for ampitude method is

better as compared to the circuit used for frequency method.

- The energy harvester unit designed is capable of delevering 3.3 V, 156 mA for a minimum line current of 50 A.

7. Acknowledgment

8. References

1. Morgan VT. The thermal rating of overhead- line conductors, Part II. A sensitivity analysis of the parameters in the steady- state thermal mode. Electr Power Syst Res. 1983; 6:287–300. https://doi.org/10.1016/0378-7796(83)90040-8

2. Morgan VT. The thermal rating of overhead- line conductors. 1. The steady- state thermal mode. Electr Power Syst Res. 1982; 5(2):119–39. https://doi.org/10.1016/0378-7796(82)90033-5

3. Overhead transmission line ampacity ratings. American Transmission Company. CR-0061v07; 2012.

4. Aluminum Electrical Conductor Handbook. The Aluminum Association. 3rd ed.; 1989.

5. Current carrying capacity of overhead transmission line ACSR conductor. Uttar Pradesh Power Transmission Corporation Limited. Available from: http://www.upptcl.org/tech_info/current_carrying.htm

6. Sathaye J, Dale L, Larsen P, Fitts G, Koy K, Lewis S, Lucena A. Estimating risk to California Energy Infrastructure from Projected Climate Change. CEC Publication CEC-500-2012-057; 2011.

7. IEEE Standard for Calculating the Current-Temperature Relationship of Bare Overhead Conductors. IEEE Std 738-2012; 2013.

8. Lindberg E. The overhead line sag dependence on weather parameters and line current. UPTEC W11 017; 2011 Dec.

9. Elisabeth Lindberg , The Overhead Line Sag Dependence on Weather Parameters and Line Current, UPTEC W11 017 December 2011.

10. Pan M-S dan, Tseng Y-C. ZigBee wireless sensor networks and their applications, Sensor Network and Configuration. Fundamentals. Techniques, Platforms, and Experiments. Springer-Verlag; 2007.

11. Datasheet Pic16F1936. Available from: http://www.microchip.com/www.products/en/PIC16F1936

12. Hoffmann K. Applying the Wheatstone Bridge Circuit. Darmstadt, Germany: Hottinger Baldwin Messtechnik GmbH; 2001.

13. Datasheet Tarang UT-20 module. Available from: https://fccid.io/document.php?id=1723546

14. Roscoe NM, Judd MD. Harvesting energy from magnetic fields to power condition monitoring sensors. IEEE Sensors Journal. 2013 Jun; 13(6):2263–70. https://doi.org/10.1109/JSEN.2013.2251625

15. Moghe R, Divan D, Lambert F. Powering low- cost utility sensors using energy harvesting, power electronics and applications (EPE 2011). Proceedings of the 2011, 14th European Conference; 2011 Aug 30-Sept 1. p. 1–10.

16. USi inductive harvester. Power Donut 2. Available from: http:/www.USi-Power.com

17. Bhuiyan RH, Dougal RA. Ali M. A miniature energy harvesting device for wireless sensors in electric power system. IEEE Sensors Journal. 2010; 10(7):1249–58. https://doi.org/10.1109/JSEN.2010.2040173

18. Chang K, Kang S, Park K, Shin S, Kim H- S. Kim H. Electric field energy harvesting powered wireless sensors for smart grid. Journal of Electrical Engineering and Technology. 2012; 7(1):75–80. https://doi.org/10.5370/JEET.2012.7.1.75

19. Guo F, Hayat H, Wang J. Energy harvesting devices for high voltage transmission line monitoring. IEEE Power and Energy Society General Meeting. 2011. p. 1–8. https://doi.org/10.1109/PES.2011.6039037

20. Musavi M, Chamberlain D, Li Q. Overhead conductor dynamic thermal rating measurement and prediction. 2011 IEEE International Conference on Smart Measurements of Future Grids (SMFG) Proceedings; Bologna. 2011. p. 135–8.

21. Gilbert JM, Balouchi F. Comparison of energy harvesting systems for wireless sensor networks. International Journal of Automation and Computing. 2008; 5(4):334–47. https://doi.org/10.1007/s11633-008-0334-2

22. Williams CB, Yates RB. Analysis of a micro-electric generator for Microsystems. Proceedings of the Transducers 95/Eurosensors IX; 1995. p. 369–72. https://doi.org/10.1109/SENSOR.1995.717207

23. Roundy S, Wright PK, Rabaey J. A study of low level vibrations as a power source for wireless sensor nodes. Computer Communications. 2003; 26(11):1131–44. https://doi.org/10.1016/S0140-3664(02)00248-7

24. Zungeru AM, Ang L, Prabaharan SRS, Seng KP. Radio frequency energy harvesting and management for wireless sensor networks. Venkataraman H, Munteam G, editors. Green Mobile Devices and Networks- Energy Optimization and Scavenging Techniques. Boca Raton, Florida: CRC Press; 2012. https://doi.org/10.1201/b10081-16